

Molecular contributions to thermo-osmotic phenomena for an electrolyte at a charged surface

Mehdi Ouadfel, Michael De San Feliciano, Cecilia Herrero,^{a)} Samy Merabia, and Laurent Joly^{b)}

Univ Lyon, Univ Claude Bernard Lyon 1, CNRS, Institut Lumière Matière, F-69622, VILLEURBANNE, France

(Dated: 30 November 2022)

Thermo-osmotic flows – generated at liquid-solid interfaces by thermal gradients – can be used to produce electric currents from waste heat on charged surfaces. The two key parameters controlling the current are the surface charge and the interfacial enthalpy excess due to liquid-solid interactions. While it has been shown that the contribution from water to the enthalpy excess can be critical, how this contribution is affected by surface charge remained to be understood. Here we use molecular dynamics simulations to investigate the impact of surface charge density on the interfacial enthalpy excess, for different distributions of the surface charge, and two different wetting conditions. We observe that surface charge has a strong impact on enthalpy excess, and that the dependence of enthalpy excess on surface charge depends largely on the surface charge distribution. In contrast, wetting has a very small impact on the charge-enthalpy coupling. We rationalize the results with simple analytical models, which can be used as guidelines to search for systems providing optimal waste heat recovery performance.

I. INTRODUCTION

Nanofluidic systems – natural porous materials and synthetic devices where liquids are confined at the nanoscale – offer great promises to address societal challenges related to water and to energy harvesting¹⁻³. Liquid-solid interfaces play a critical role in such nanoscale systems, and surface effects provide efficient means to produce electricity from various thermodynamic gradients available in nature. For instance, diffusio-osmotic flows – generated at liquid-solid interfaces under a gradient of salt concentration – can be used to produce electricity from the salinity difference between sea and river water, the so-called blue energy harvesting⁴⁻⁶. Indeed, if the solid surface is charged, the liquid will bear an opposite charge carried by ions, which will be advected by the osmotic flow and result in an electrical current.

Similarly, thermo-osmotic flows⁷⁻¹¹ – induced by thermal gradients – could be used to produce electricity from low-grade waste heat¹²⁻¹⁴. The electric current produced is controlled by the surface charge – opposite to the charge in the liquid, and by the velocity of the osmotic flow. A key parameter controlling the thermo-osmotic flow velocity is the interfacial enthalpy excess, arising from the interactions of the liquid with the solid^{15,16}. It has been shown recently that in addition to the commonly considered ion electrostatic contribution to the enthalpy excess^{17,18}, the contribution from water could also be significant, and even dominate over the ionic one^{14,19}. While the ion contribution is well described by the Poisson-Boltzmann framework²⁰ (especially at low salt concentrations, at which this contribution becomes

large), the water contribution results from specific interactions with the surface and requires descriptions at the molecular level, for instance with molecular dynamics simulations.

However, previous studies have only computed the water enthalpy excess on charge neutral surfaces¹⁹. With the ultimate goal to use thermo-osmosis to produce electricity, it is crucial to understand how surface charge modifies the interfacial enthalpy excess, and in particular its water contribution. This is the objective of this article, where we present the results of molecular dynamics simulations of an aqueous electrolyte confined between parallel charged walls. We used a large salt concentration, so that the ion contribution is negligible as compared to the one of water. We investigated the impact of surface charge density on the interfacial enthalpy excess, for different distributions of the surface charge, and two different wetting conditions. We rationalized the results with simple analytical models, which can be used to evaluate the interfacial enthalpy excess in a wide variety of systems.

II. METHODS

A. Channel model

We used the LAMMPS package²¹ to perform equilibrium molecular dynamics simulations of an aqueous electrolyte composed of 2000 water molecules and NaCl salt with a bulk concentration $n_s \sim 0.20$ M, for a Debye length $\lambda_D \sim 7$ Å, confined between two parallel walls made of four atomic layers of a fcc crystal with a lattice parameter $a = 5.3496$ Å. We applied periodic boundary conditions in the x and y directions for our system of size $L_x = L_y = 32.0976$ Å. Water molecules were simulated using the SPC/E model²², in which the atomic interactions are modeled with a Lennard-Jones (LJ) potential defined by σ_{ii} the characteristic diameter and ϵ_{ii} the in-

^{a)}Currently at Laboratoire Charles Coulomb (L2C), Université de Montpellier, CNRS, 34095 Montpellier, France

^{b)}Electronic mail: laurent.joly@univ-lyon1.fr

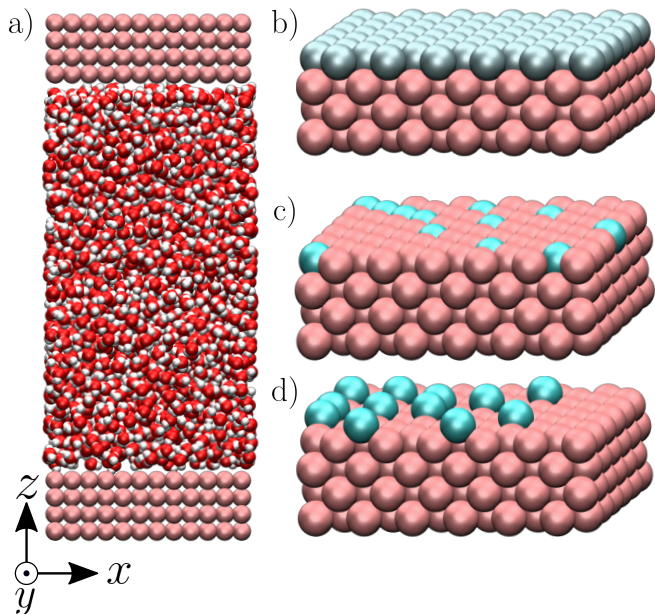


FIG. 1. Visualization of the modeled systems composed of an aqueous electrolyte solution confined between two walls (a) realized with VMD²⁵. The walls are charged either homogeneously (b), heterogeneously (c) or with the charge overhanging the walls to create the 'defect' case (d) (see text for more details).

teraction energy of particle i , and a Coulombic potential. For the ions, we used the LJ parameters given in Ref. 23 along with the Lorentz-Berthelot mixing rules. As for the LJ wall, we chose the parameters to have either a hydrophobic or a hydrophilic surface, following Ref. 24. We studied three types of surface charge: 1. A homogeneous case where we charged all surface atoms with a charge $q = \Sigma / (SN_{\text{wall}})$, where $S = L_x L_y$ is the surface of the wall and N_{wall} the number of atoms on the surface, which results in a surface charge density Σ (Fig. 1.b). 2. A heterogeneous case where we selected atoms of the surface randomly and gave them a charge of $\pm 1 e$ (Fig. 1.c) so that the surface charge density was Σ . 3. A case in which atoms with a charge of $\pm 1 e$ protrude from the surface with respect to the fcc structure of the crystal. The charges are placed on top of the wall, simulating defect on the surface (Fig. 1.d). Counter-ions were added to the system to keep it electrically neutral. The bottom wall was frozen and we used the top wall as a rigid piston during an equilibration phase that lasted 0.6 ns, before fixing it at its equilibrium position to set the pressure to 10 atm, following previous studies^{19,24}. The equilibrium distance between the walls was $h \sim 60 \text{ \AA}$. We fixed the temperature of the fluid at 298 K via a Nosé-Hoover thermostat with a damping time of 100 fs. The simulations lasted for 10 ns with a timestep of 2 fs.

B. Quantities of interest

For a mixture of particles, we define the enthalpy excess density as²⁶:

$$\delta h(z) = \sum_i n_i(z) [h_i - h_i^B], \quad (1)$$

with $i \in [\text{O}, \text{H}, \text{Na}, \text{Cl}]$ the atom type, n_i the atomic density and h_i the enthalpy per particle. The index B refers to a bulk quantity, i.e. far from the surface, where it is homogeneous and isotropic. We defined the enthalpy per particle as:

$$h_i(z) = u_i(z) + \frac{p^{\parallel}(z)}{n_{\text{tot}}(z)}, \quad (2)$$

where u_i is the internal energy per particle, $n_{\text{tot}}(z) = \sum_i n_i(z)$ the total number density and $p^{\parallel}(z)$ the components of the virial pressure tensor parallel to the surface (p^{xx} or p^{yy} , which are equal). Indeed, pressure is anisotropic near the wall, and following previous studies^{26,27}, we consider the pressure component parallel to the surface to compute the enthalpy excess density. We can consider only the contribution of the potential energy to calculate the internal energy term. Indeed the equipartition theorem shows us that the kinetic energy terms cancel out: $u_k(z) = u_k^B$. Here attributing $p^{\parallel}(z)/n_{\text{tot}}(z)$ to each atom amounts to evenly distribute the atomic volume regardless of the atom type. We finally obtain the expression of the enthalpy excess density:

$$\delta h(z) = \sum_i n_i(z) [u_{p,i}(z) - u_{p,i}^B] + p^{\parallel}(z) - \frac{p^B}{n_{\text{tot}}^B} n_{\text{tot}}(z), \quad (3)$$

where we denote p^B the bulk pressure, which is isotropic.

We compute pressure profiles using the stress per atom. Indeed the virial part of the stress per atom is given by $\Pi_i^{\alpha\beta} = -\sum_k^{N_i} r_{k\alpha} f_{k\beta}$ where α and $\beta \in \{x, y, z\}$, and N_i is the number of atoms of type i . With this definition, $p_{\alpha\beta}(z) = -(1/V) \sum_i \Pi_i^{\alpha\beta}(z)$. Finally, we can compute the enthalpy excess by integrating the enthalpy excess density from the wall surface (i.e. the position of the atoms on the surface) to the middle of the channel: $\Delta H = \int_{\text{wall}}^{\text{middle}} \delta h(z) dz$, which we decompose into three contributions: the water internal energy excess ΔU_{water} , the ions internal energy excess ΔU_{ions} and a pressure excess term ΔP^{\parallel} :

$$\Delta U_{\text{water}} = \int_{\text{wall}}^{\text{middle}} \{n_{\text{O}}(z) [u_{p,\text{O}}(z) - u_{p,\text{O}}^B] + n_{\text{H}}(z) [u_{p,\text{H}}(z) - u_{p,\text{H}}^B]\} dz \quad (4)$$

$$\Delta U_{\text{ions}} = \int_{\text{wall}}^{\text{middle}} \{n_{\text{Na}}(z) [u_{p,\text{Na}}(z) - u_{p,\text{Na}}^B] + n_{\text{Cl}}(z) [u_{p,\text{Cl}}(z) - u_{p,\text{Cl}}^B]\} dz \quad (5)$$

$$\Delta P^{\parallel} = \int_{\text{wall}}^{\text{middle}} \left[p^{\parallel}(z) - \frac{p^B}{n_{\text{tot}}^B} n_{\text{tot}}(z) \right] dz. \quad (6)$$

III. RESULTS AND DISCUSSION

Figure 2 presents the enthalpy excess ΔH and its contributions as a function of the surface charge density. One can observe that ΔH varies notably with Σ , increasing significantly with the absolute value of the surface charge density. Even at the large salt concentration considered here and at large surface charges, ions do not have much impact on the enthalpy excess. This is due to their presence in small quantities in the system as compared to water molecules. It is actually ΔU_{water} and ΔP^{\parallel} which drive the enthalpy excess.

Let us first focus on ΔU_{water} : the water energy term has a parabolic form, which is relatively symmetrical with the surface charge density. One can approximate this quantity by a simple dipole model. In fact, at the interface the water molecules orient themselves under the effect of the electric field created by the charged wall. In this regard the energy excess density $\delta u_{\text{water}}^{\text{dp}}$ can be expressed as:

$$\delta u_{\text{water}}^{\text{dp}}(z) = -\langle \mu_z \rangle(z) n_{\text{O}}(z) E(z), \quad (7)$$

with n_{O} the number density of oxygen atoms, $E(z) = \Sigma/\epsilon_0\epsilon_r$ the electrostatic field, and $\langle \mu_z(z) \rangle = \mu \langle \cos(\theta)(z) \rangle$ the average dipole moment along the z axis, with $\langle \cos(\theta) \rangle$ the average dipole moment orientation and θ the angle formed by the dipole with the surface, and $\mu = 1.85$ D the water dipole moment. In the electrical double layer (EDL), which is a layer of electrically charged liquid that screens the electric field created by a charged wall, the electric field is weak and δu^{dp} is negligible¹⁹. However, for water molecules in the first two interfacial layers, the perpendicular (or out-of-plane) relative permittivity ϵ_{\perp} is greatly reduced^{28,29}. This reduction is due to the preferential orientation of water molecules close to the wall along the z direction, which reduces the polarizability of water and thus the dielectric constant in this direction. The electric field becomes stronger and δu^{dp} is not negligible anymore. We can compute $\langle \cos(\theta) \rangle$ from the simulation or we can compute it theoretically using Boltzmann statistics (Fig. 3.b). Let $P(\theta)$ be the probability for a molecule to have an orientation angle θ , we have:

$$P(\theta) = \frac{e^{\alpha \cos(\theta)}}{\int e^{\alpha \cos(\theta)} d\Omega}, \quad (8)$$

with Ω the solid angle and $\alpha = \beta\mu E$ with $\beta = 1/k_B T$. Thus,

$$\langle \cos(\theta) \rangle = \int P(\theta) \cos(\theta) d\Omega = \coth(\alpha) - \frac{1}{\alpha}. \quad (9)$$

As stated before, near the interface, the relative permittivity decreases significantly and we can no longer consider the bulk value $\epsilon_r = 71$ for SPC/E water^{30,31}. This is why we considered an effective relative permittivity ϵ_r^{eff} , treated as a fitting parameter. Thus, writing

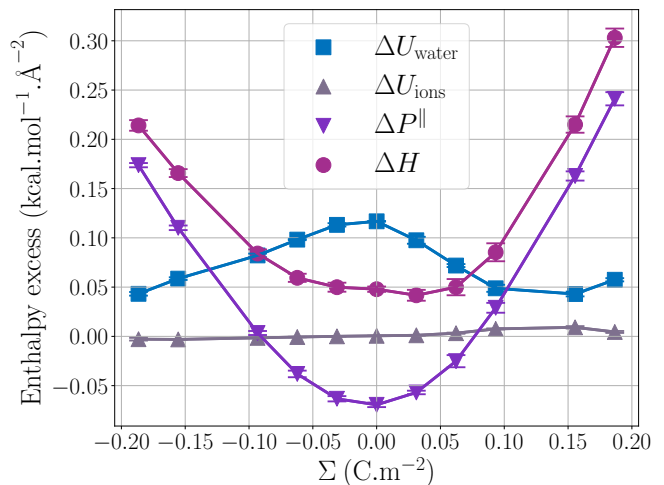


FIG. 2. Comparison of the contributions to ΔH (mauve circles): ΔU_{ions} (grey triangles up) the contribution of the potential energy of the ions, ΔU_{water} (blue squares) the contribution of the water potential energy and ΔP^{\parallel} (purple triangles down) the pressure excess. One can observe that the enthalpy excess varies drastically with the surface charge density, increasing by a factor of 4 to 6 for the highest surface charge densities considered.

$E = \Sigma/\epsilon_0\epsilon_r^{\text{eff}}$, one obtains:

$$\delta u_{\text{water}}^{\text{dp}} = -\frac{\mu \left(\coth(\alpha) - \frac{1}{\alpha} \right) \Sigma}{\epsilon_0\epsilon_r^{\text{eff}}} n_{\text{O}}(z), \quad (10)$$

and so:

$$\Delta U_{\text{water}}^{\text{dp}} = -\frac{\mu \left(\coth(\alpha) - \frac{1}{\alpha} \right) \Sigma}{\epsilon_0\epsilon_r^{\text{eff}}} n_{\text{O}}^{\text{surf}}, \quad (11)$$

with $n_{\text{O}}^{\text{surf}}$ the atomic surface density of the first layer, which can be computed from the simulations. Finally $\Delta U_{\text{water}} = \Delta U_{\text{water}}^0 + \Delta U_{\text{water}}^{\text{dp}}$, where $\Delta U_{\text{water}}^0$ is the value of ΔU_{water} for a neutral surface.

Fig. 3.b represents the dipole orientation, measured and computed. We can see an asymmetry of the measured curve, the dipole orientation follows two different patterns: for the negative charge surfaces, θ precisely follows its theoretical value by taking $\epsilon_r^{\text{eff}} = 12$. However, for the positive ones, the model is less accurate. To fit this part of the curve, we took $\epsilon_r^{\text{eff}} = 9$. As mentioned above, the dielectric constant of the first layers depends on water molecules orientation. Its asymmetric behavior, depending on the sign of the surface charge density, is therefore not unexpected. Figure 3.c presents the atomic surface density of the first layer, measured and theoretical where $n_{\text{O}}^{\text{surf}}$ can be approximated by $1/\sigma_{\text{O}}^2$ with σ_{O} the oxygen LJ diameter. We thus have two ways of plotting the model presented (Fig. 3.a): from direct measurement of $\langle \cos(\theta) \rangle$ and $n_{\text{O}}^{\text{surf}}$, or from their theoretical values. Although the asymmetry of $\cos(\theta)$ and $n_{\text{O}}^{\text{surf}}$ is not sufficient

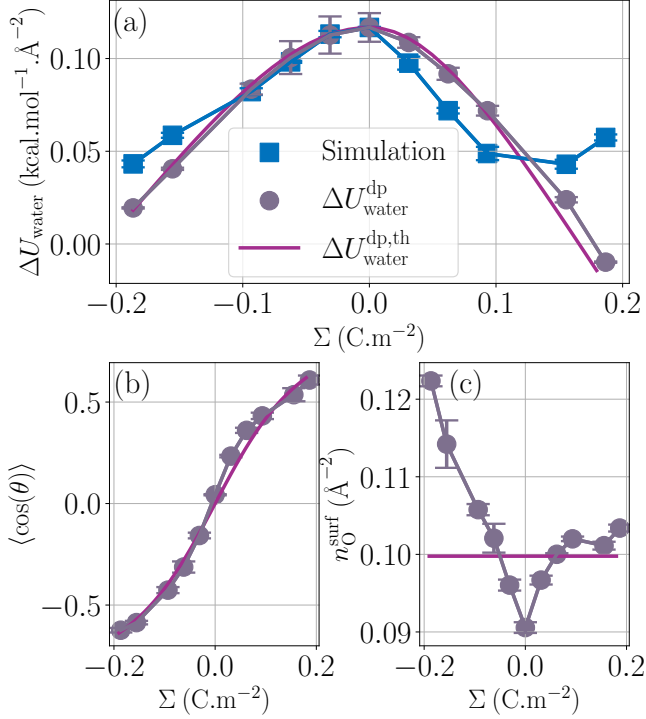


FIG. 3. Water contribution to the enthalpy excess (a) with the measured values ΔU_{water} (blue squares), the theoretical model with measured $\langle \cos(\theta) \rangle$ and $n_{\text{O}}^{\text{surf}}$ (grey circles), and the fully theoretical model (mauve). The theoretical and measured orientation of water molecules near the surface (respectively mauve line and grey circles) is given in (b). The effective permittivity was set to $\epsilon_r^{\text{eff}} = 12$ for negative charge surface density and $\epsilon_r^{\text{eff}} = 9$ for positive charge. The surface density of water molecules near the interface is given in (c) with the same legend as (b).

to explain the one found in ΔU_{water} , overall our model describes fairly the water excess energy.

Regarding the pressure term, one way to approach it is to compute the excess perpendicular pressure ΔP^{\perp} and then calculate ΔP^{\parallel} using the surface tension γ . Indeed the mechanical route to define the surface tension is³²:

$$\gamma = \int_{\text{wall}}^{\text{middle}} [p_{\perp} - p_{\parallel}] dz \quad (12)$$

$$= \Delta P^{\perp} - \Delta P^{\parallel}, \quad (13)$$

where p_{\perp} and p_{\parallel} are the normal and tangential components of the pressure tensor. Using Eq. (13), we can determine ΔP^{\parallel} from γ and ΔP^{\perp} .

The variation of the surface tension with the wall surface charge is given by the Lippmann's equation^{33,34}, which considers the energy stored in the capacitor formed by the charged surface and the EDL:

$$\gamma = \gamma_0 - \frac{\Sigma^2}{2C} = \gamma_0 - \frac{d\Sigma^2}{2\epsilon_0\epsilon_r^{\text{eff}}}, \quad (14)$$

where γ_0 is the surface tension for a neutral surface and $C = \epsilon_0\epsilon_r^{\text{eff}}/d$ is the capacitance per unit area, with d

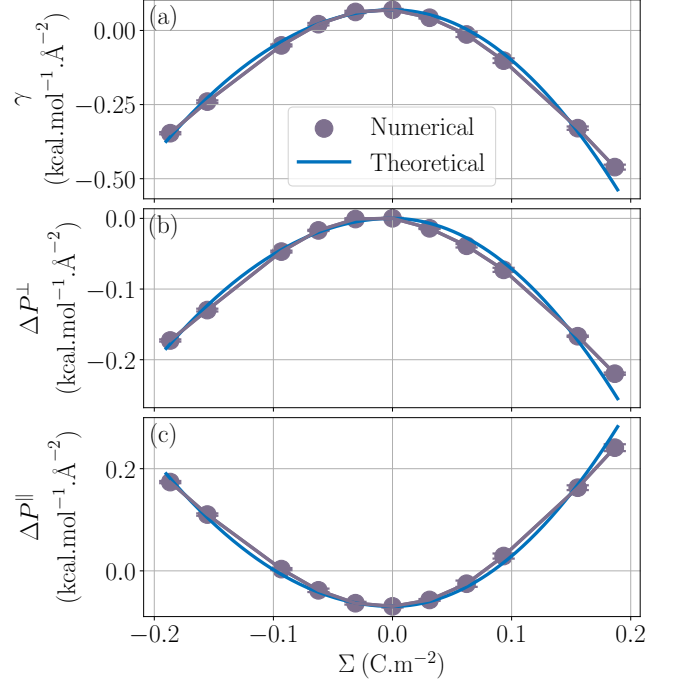


FIG. 4. Pressure term ΔP^{\parallel} determined with the surface tension γ and the perpendicular pressure ΔP^{\perp} using a capacitor model.

the capacitor thickness, i.e. the mean distance between charges on the wall and counter-ions in the EDL. Again, the relative permittivity ϵ_r^{eff} used in the model must be smaller than the one of bulk water due to its drop near the interface. Moreover the capacitor thickness d is unknown so the right way to fit the capacitor model with our values is to adjust C . In addition we can see in Fig. 3.c that near the surface, water displays different structure depending on the sign of Σ , and so should do d . This allows us to fit our model with two values of the capacitance C , one for the negative charge surfaces and another one for positive ones (Tab. I). A way to apprehend these capacitance is to look at their corresponding relative permittivity when fixing the capacitor thickness. The values of Tab. I were computed using $d = 5 \text{ \AA}$ and one can note that they remain consistent with our previous discussion on the drop of ϵ_r near the interface.

For the perpendicular pressure, its variation with the surface charge comes from the electrostatic pressure created by the capacitor³⁵. Integrating it over the length of the capacitor give us the following expression:

$$\Delta P^{\perp} = \Delta P^{\perp, \Sigma=0} - \frac{\Sigma^2}{2C}, \quad (15)$$

where $\Delta P^{\perp, \Sigma=0}$ is the perpendicular pressure excess for a neutral surface. Again, we can fit it using different capacitance depending on the sign of the surface charge density (Tab. I). Note that the effective relative permittivity is different for γ and for ΔP^{\perp} . Our assumption is that this is a consequence of the anisotropy of ϵ_r near

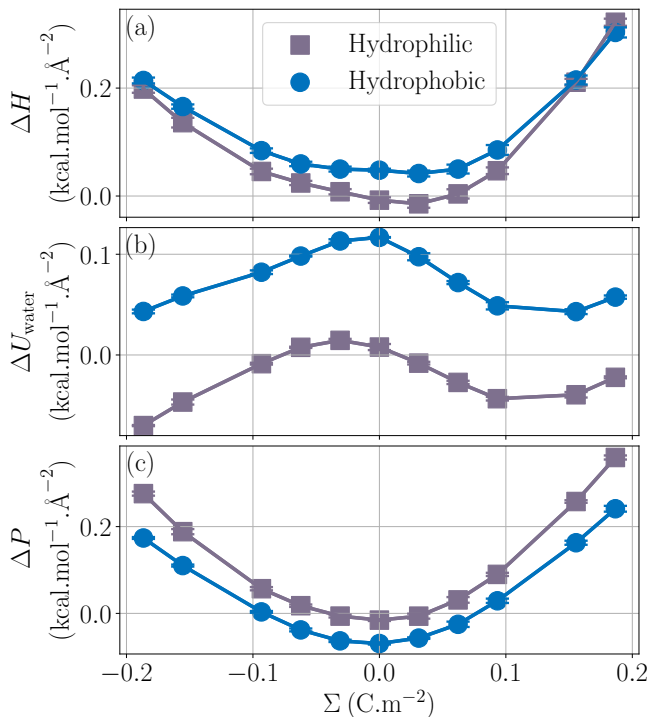


FIG. 5. Impact of wetting on the enthalpy excess (a) with the hydrophobic case (blue circles) and the hydrophilic case (grey squares) with the water contribution (b) and the pressure contribution (c). One can note that there is not much of a qualitative effect of the wetting to ΔH .

the interface. γ is indeed a function of ΔP^\perp and ΔP^\parallel , so the relative permittivity used in the capacitor model should depend on both parallel and perpendicular components of the permittivity tensor, resulting in different ϵ_r^{eff} for γ and ΔP^\perp . We are finally able to determine $\Delta P^\parallel = \Delta P^\perp - \gamma$ (Fig.4.c). One can note that the surface tension dominates the pressure term by a factor of 2 in the expression of ΔP^\parallel , which gives it its parabolic form.

C (F.m^{-2})	$\Sigma < 0$	$\Sigma > 0$
γ	0.053	0.039
ΔP^\perp	0.141	0.100
$\epsilon_r^{\text{eff}}(\gamma)$	3.0	2.2
$\epsilon_r^{\text{eff}}(\Delta P^\perp)$	8.0	5.7

TABLE I. Capacitance per unit area C and the resulting ϵ_r^{eff} by taking a fixed capacitor thickness $d = 5 \text{ \AA}$, for the different capacitor models.

Now that we have understood the behavior of the enthalpy excess for a hydrophobic and homogeneously charged wall, let us look at the effect of wetting and charge distribution on the enthalpy excess. In Fig. 5.a we compared the enthalpy excess of a hydrophobic and a hydrophilic surface. It appears that there is a small quantitative difference between the two wettings and one

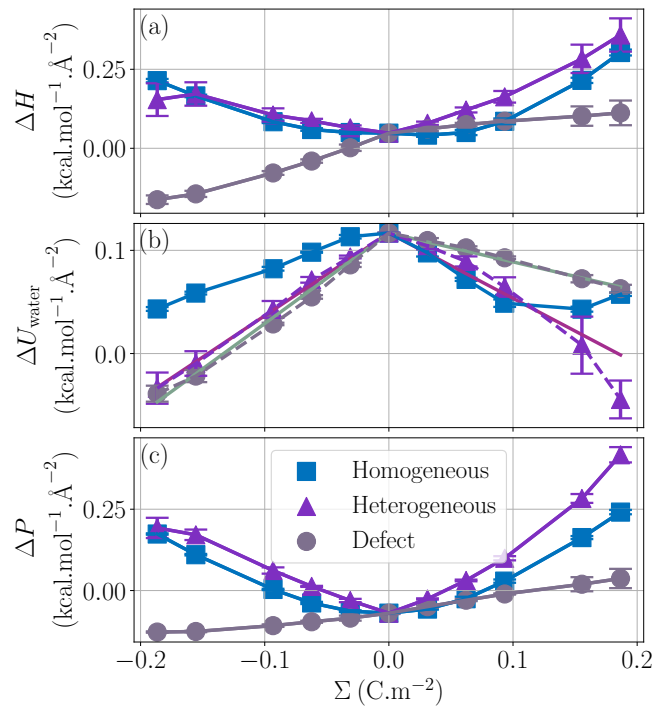


FIG. 6. Effects of the charge distribution on the enthalpy excess. We can see a change of behavior of ΔH with the defect case, taking negative values for negatively charge surface. For ΔU_{water} (b), the homogeneous case (blue squares) is described by a dipole model while the other ones are described by a linear model of potential energy excess per unit charge. For ΔP^\parallel (c), the homogeneous as well as the heterogeneous case can be described by a capacitor model but the model cannot describe the defect case.

can say as a first approximation that the wetting simply shifts the values of ΔH . The enthalpy excess is found to be smaller in the hydrophilic case. When looking at the decomposition of the enthalpy excess it appears that ΔU_{water} is simply shifted and becomes smaller. Water molecules are indeed more attracted to the wall in the hydrophilic case, which allows them to adopt a more favorable energy configuration thus reducing the overall internal energy (figure 5.b). The pressure term is also shifted and the parabola is more pronounced. One can use the capacitor model to understand this: in the hydrophilic case, water molecules are closer to the surface, thus the capacitor is thinner, resulting in a variation of the capacitance and a modification of the curvature of ΔP^\parallel . Note that we simulated two systems with very different wetting properties, and the change in capacitance remained minimal, so that considering that the capacitance is independent of wetting represents a good approximation.

Regarding the charge distribution, one can see in Fig. 6 that this has a drastic impact on the enthalpy excess. In particular, the defect case displays a different behavior than the other two, having a change of sign for negative charge surfaces. One can understand these differences

by looking at the decomposition of ΔH . For ΔU_{water} (Fig. 6.b), the dipole model, which assumes a homogeneous charge distribution, does not work for the heterogeneous and defect cases. In heterogeneous cases, a charge will only affect the surrounding water molecules. Indeed, with a heterogeneous charge distribution, a counter-ion will tend to bond to each charge with the effect to screen the electric field. Thus the effect of charges is local and it is independent of one another. Therefore the variation of the energy excess is simply proportional to the number of surface charges:

$$\Delta U_{\text{water}} = \Delta U_{\text{water}}^{\Sigma=0} + U^{\text{ES}} \frac{\Sigma}{e} \quad (16)$$

where U^{ES} is the energy excess per charge and is a function of $\text{sgn}(\Sigma)$ and the charge distribution (table II), and e is the elementary charge.

U^{ES} (kcal.mol ⁻¹)	$\Sigma < 0$	$\Sigma > 0$
Heterogeneous	1.24e - 2	-9.8e - 3
Defect	1.32e - 2	-4.3e - 3

TABLE II. Water enthalpy excess per charge for different charge distributions.

Even though there is a quantitative difference between the three cases for ΔU_{water} , the differences on the enthalpy excess come largely from ΔP^{\parallel} (Fig. 6.c). For the heterogeneously charged surface, even though the charge is not evenly distributed, the capacitor model is still applicable, due to the presence of a clear gap between water molecules and the surface. However, in the presence of defects, water molecules near the surface are on the same level as charges. In this case, the thickness of the capacitor d is 0, and our model predicts that the parabolic dependence of ΔP^{\parallel} with Σ should vanish. We suggest that the small remaining drift of ΔP^{\parallel} with the surface charge, not captured by our model, originates from specific liquid-wall interactions, indirectly affected by the surface charge.

IV. CONCLUSION

In this article, we used equilibrium molecular dynamics simulations to study the effect of surface charge density and charge distribution on the enthalpy excess, a key parameter involved in thermo-osmotic phenomena. We have shown that the surface charge density has a large impact on the enthalpy excess. For homogeneously charged surfaces, the enthalpy excess is enhanced by 300 to 500 % for the highest surface charge densities considered. This is due to the amplitude of the pressure variations near the wall, which increase with the absolute value of the surface charge density. We then studied the effect of wetting to realize that it does not significantly modify the impact of surface charge on the enthalpy excess. Nonetheless the values of the enthalpy excess are more important in

the hydrophobic case, especially at small surface charges, it is thus preferable to use this type of wetting to maximize the enthalpy excess. We also studied the effect of the charge distribution on the enthalpy excess. We have shown that using homogeneously or heterogeneously charged surfaces has no real influence on the enthalpy excess. However, the presence of protruding defects has a great influence on it. In particular, with this charge distribution we have been able to observe a change of sign of ΔH for negative surface charges. Overall we provide a useful tool to explore wide variety of systems and identify those promising the best thermo-osmotic performance, without the need to use non-equilibrium molecular dynamics. For example it could be interesting to study new two-dimensional materials with this method.

ACKNOWLEDGMENTS

This work is supported by the ANR, Project ANR-21-CE50-0042-01 smoothE.

V. REFERENCES

- ¹R. Schoch, J. Han, and P. Renaud, *Reviews of Modern Physics* **80**, 839 (2008).
- ²L. Bocquet and E. Charlaix, *Chem. Soc. Rev.* **39**, 1073 (2010).
- ³N. Kavokine, R. R. Netz, and L. Bocquet, *Annual Review of Fluid Mechanics* **53**, 377 (2021).
- ⁴A. Siria, M.-L. Bocquet, and L. Bocquet, *Nature Reviews Chemistry* **1**, 0091 (2017).
- ⁵S. Marbach and L. Bocquet, *Chemical Society Reviews* **48**, 3102 (2019).
- ⁶L. Joly, R. H. Meißner, M. Iannuzzi, and G. Tocci, *ACS Nano* **15**, 15249 (2021).
- ⁷A. P. Bregulla, A. Würger, K. Günther, M. Mertig, and F. Cichos, *Physical Review Letters* **116**, 188303 (2016).
- ⁸L. Fu, S. Merabia, and L. Joly, *Physical Review Letters* **119**, 214501 (2017).
- ⁹V. M. Barragán and S. Kjelstrup, *Journal of Non-Equilibrium Thermodynamics* **42**, 217 (2017).
- ¹⁰K. Proesmans and D. Frenkel, *The Journal of Chemical Physics* **151**, 124109 (2019).
- ¹¹P. Anzini, G. M. Colombo, Z. Filiberti, and A. Parola, *Physical Review Letters* **123**, 028002 (2019).
- ¹²M. Dietzel and S. Hardt, *Physical Review Letters* **116**, 225901 (2016).
- ¹³M. Dietzel and S. Hardt, *Journal of Fluid Mechanics* **813**, 1060 (2017).
- ¹⁴L. Fu, L. Joly, and S. Merabia, *Physical Review Letters* **123**, 138001 (2019).
- ¹⁵J. Anderson, *Annual Review of Fluid Mechanics* **21**, 61 (1989).
- ¹⁶C. Herrero, A. Allemand, S. Merabia, A.-L. Biance, and L. Joly, arXiv preprint arXiv:2204.13522 (2022).
- ¹⁷B. V. Derjaguin and G. P. Sidorenkov, *CR Acad. Sci. URSS* **32**, 622 (1941).
- ¹⁸B. V. Derjaguin, N. V. Churaev, V. M. Muller, and V. Kisin, *Surface forces* (Springer, 1987).
- ¹⁹C. Herrero, M. De San Feliciano, S. Merabia, and L. Joly, *Nanoscale* **14**, 626 (2022).
- ²⁰C. Herrero and L. Joly, arXiv preprint arXiv:2105.00720v2 (2022).

- ²¹A. P. Thompson, H. M. Aktulga, R. Berger, D. S. Bolintineanu, W. M. Brown, P. S. Crozier, P. J. in 't Veld, A. Kohlmeyer, S. G. Moore, T. D. Nguyen, R. Shan, M. J. Stevens, J. Tranchida, C. Trott, and S. J. Plimpton, *Comp. Phys. Comm.* **271**, 108171 (2022).
- ²²H. J. C. Berendsen, J. R. Grigera, and T. P. Straatsma, *The Journal of Physical Chemistry* **91**, 6269 (1987), <https://doi.org/10.1021/jp100308a038>.
- ²³S. Koneshan, J. C. Rasaiah, R. M. Lynden-Bell, and S. H. Lee, *The Journal of Physical Chemistry B* **102**, 4193 (1998), <https://doi.org/10.1021/jp980642x>.
- ²⁴D. M. Huang, C. Cottin-Bizonne, C. Ybert, and L. Bocquet, *Phys. Rev. Lett.* **98**, 177801 (2007).
- ²⁵W. Humphrey, A. Dalke, and K. Schulten, *Journal of Molecular Graphics* **14**, 33 (1996).
- ²⁶R. Ganti, Y. Liu, and D. Frenkel, *Phys. Rev. Lett.* **119**, 038002 (2017).
- ²⁷P. Anzini, Z. Filiberti, and A. Parola, *Phys. Rev. E* **106**, 024116 (2022).
- ²⁸H. Itoh and H. Sakuma, *The Journal of Chemical Physics* **142**, 184703 (2015).
- ²⁹T. Dufils, C. Schran, J. Chen, A. K. Geim, L. Fumagalli, and A. Michaelides, *Understanding the anomalously low dielectric constant of confined water: an ab initio study* (2022), arXiv:2211.14035 [physics].
- ³⁰M. Rami Reddy and M. Berkowitz, *Chemical Physics Letters* **155**, 173 (1989).
- ³¹D. Braun, S. Boresch, and O. Steinhauser, *The Journal of Chemical Physics* **140**, 064107 (2014), <https://doi.org/10.1063/1.4864117>.
- ³²C. Vega and E. de Miguel, *The Journal of Chemical Physics* **126**, 154707 (2007), <https://doi.org/10.1063/1.2715577>.
- ³³G. Lippmann, *Relations entre les phénomènes électriques et capillaires* (Gauthier-Villars, 1875).
- ³⁴D. Kramer and J. Weismüller, *Surface Science* **601**, 3042 (2007).
- ³⁵F. Mugele and J.-C. Baret, *Journal of Physics: Condensed Matter* **17**, R705 (2005).